JOURNAL OF CATALYSIS 114, 8–16 (1988)

Selective Synthesis of Dimethylamine over Small-Pore Zeolites

II. Effects of Impurities on Catalytic Properties of H-RHO

R. D. SHANNON, M. KEANE, JR., L. ABRAMS, R. H. STALEY, T. E. GIER, D. R. CORBIN, AND G. C. SONNICHSEN

Central Research and Development Department,[1] E. I. du Pont de Nemours & Company, Experimental Station, Wilmington, Delaware 19898

Received August 25, 1987; revised May 30, 1988

Typical RHO preparations can contain impurities such as unreacted gel, chabazite, P_c, and pollucite. These impurities were synthesized in pure form to investigate their effects on the behavior of RHO as a dimethylamine (DMA)-selective catalyst in the methanol–ammonia reaction. Gel and P_c, after exchange and calcination, were amorphous and inactive at typical reaction temperatures of 300–325°C. Chabazite, always present in RHO preparations at 5–10% levels, is active and DMA selective after deep-bed calcination. After shallow-bed calcination, it loses much of its crystallinity and becomes inactive. Pollucite, appearing in the later stages of RHO crystallization, loses activity at 325°C after shallow-bed calcination. However, after deep-bed calcination, it is an active and nonselective methylamine catalyst. Thus, the presence of pollucite can be a primary cause of lower DMA selectivity of deep-bed calcined RHO catalysts. Steaming, one of the most effective methods of reducing the activities of impurities, destroys pollucite crystallinity and/or nonselective surface sites.

INTRODUCTION

The unusually high activity and dimethylamine selectivity of zeolite H-RHO in the synthesis of methylamines from methanol and ammonia were recently described (*1–4*). Dimethylamine (DMA) and trimethylamine (TMA) selectivities depend not only on the method and temperature of preparation of H-RHO from the NH_4-RHO precursor (*4*), but also on the nature and amount of impurities present.

Zeolite RHO preparations can contain a variety of impurities—gel, chabazite, P_c, pollucite, and several phases of unknown structure. Gel is occasionally found if the RHO crystallization is stopped prematurely.

An impurity phase that appears irregularly at low levels during RHO crystallization has an X-ray pattern similar to that of zeolite P_c. P_c, described by Barrer *et al.* (*5, 6*) and by Taylor and Roy (*7*), is similar to gismondine, $Ca_4Al_8Si_8O_{32} \cdot 16H_2O$, a small-pore zeolite with a three-dimensional channel system having pore dimensions [3.1 × 4.4] ↔ [2.8 × 4.9 Å] (*8*). Such small-pore openings are too small for reactant absorption and therefore for selective methylamines synthesis. Synthetic Na-P_c, $Na_6Al_6Si_{10}O_{32} \cdot 12H_2O$ (*9*), with a spherulitic morphology is probably closer to the composition found as an impurity in the RHO synthesis than gismondine because of the presence of Na in typical RHO preparations.

In the later stages of RHO crystallization a phase resembling pollucite, $CsAlSi_2O_6 \cdot nH_2O$, appears. The mineral pollucite, $Cs_{12}Na_4Al_{16}Si_{32}O_{96} \cdot 4H_2O$, has the analcime structure with six-ring apertures of ~2.6 Å diameter (*10*). Pollucite concentrations increase as crystallization is carried out for longer periods.

Chabazite, nominally $(Ca, Mg, Na, K)_n Al_{12}Si_{24}O_{72} \cdot 40H_2O$, has a hexagonal or pseudohexagonal structure with eight-ring pore openings (3.6 × 3.7 Å) (*8*) similar in

[1] Contribution 4471.

0021-9517/88 $3.00

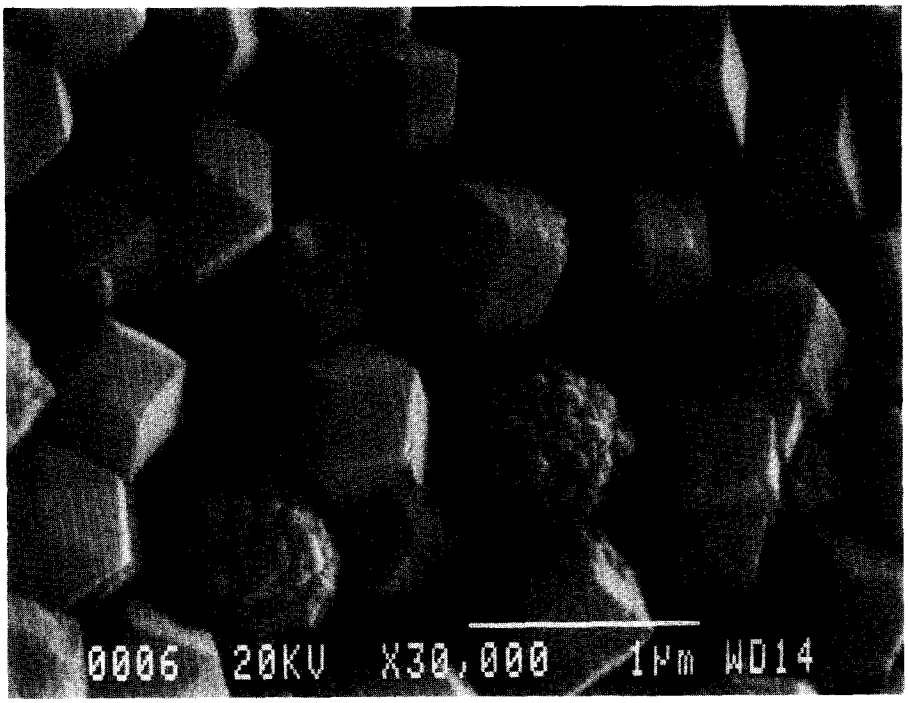

FIG. 1. Scanning electron micrographs of zeolite RHO preparations containing typical spherulitic chabazite impurities.

size to those of RHO. Chabazite crystallizes from the gel at the same time as RHO in the form of cauliflower-shaped aggregates and has been observed in all RHO preparations at 5–20% levels (see Fig. 1).

To determine the catalytic behavior of these impurities on methylamine and dimethyl ether (DME) selectivities, we have prepared gel, P_c, pollucite, and chabazite in relatively pure forms. Although these synthesized forms may not correspond exactly to the impurity phases found in a RHO preparation, this approach provides some insights into the role that these impurities play in the methylamine synthesis. This paper compares the catalytic properties of synthesized H-gel, H-chabazite, H-P_c, and H-pollucite calcined under dry shallow-bed (SBN), shallow-bed steaming (SBST), and deep-bed (DB) conditions.

EXPERIMENTAL

Gel was prepared by stopping a RHO crystallization after 24 h. K,Cs-chabazite (A) was obtained from a ZK-5 preparation (*11*) that was heated for 16 days. A sample of K-chabazite (B) was obtained from the Smithsonian Institution. Two samples of P_c (A, B) were obtained from Na_2O–Al_2O_3–SiO_2 gels at 175°C with SiO_2/Al_2O_3 = 2.68 according to the procedure of Kimpe (*12*). A third P_c(C) was prepared from a similar gel with SiO_2/Al_2O_3 = 0.6 at 95°C for 24 h.

A sample of pollucite 0.2–0.4 μm in diameter was prepared from a Na_2O–Cs_2O–Al_2O_3–SiO_2 gel at 80°C for 7 days according to the procedure of Robson (*13*). Wet chemical analysis indicated a composition of $Na_{8.7}Cs_{2.4}Al_{12.9}Si_{35.1}O_{96}$. A second sample of pollucite consisting of 1- to 3-μm-diameter spheres was prepared from a RHO preparation (*4*) carried out at 90–100°C for ~40 days.

Each of these impurity phases was exchanged four times at 80°C with 10% NH_4NO_3 solutions and calcined at 600°C using SBN, DB, or SBST calcination. The experimental details of SBN, DB, and SBST cal-

cination are described in Part I of this series (*4*). The 0.2- to 0.4-μm pollucite had the composition $[H_{9.4}]Na_{1.15}Cs_{2.2}Al_{12.8}Si_{35.2}O_{96}$, where H has been introduced for charge balance. Exchange of the 1- to 3-μm sample provided a material with the composition $[H_{14}]Na_{5.3}Cs_{4.4}Al_{11.2}Si_{36.8}O_{96}$ after four exchanges and calcination at 600°C for 4 h.

In addition to the individual impurity phases, a series of RHO samples was prepared using mixtures of 200 ml 4 *M* Na_2Al_2 OH, 56 ml 50% CsOH, and 32 g NaOH to 720 ml of colloidal silica (Ludox LS-30) in a polytetrafluoroethylene (Teflon) bottle, and allowing them to stand at 25°C for 9 days, similar to preparations described earlier (*4*). These mixtures were crystallized from 0 to 100 h to obtain increasing amounts of the impurities P_c, chabazite, and pollucite. The H forms were prepared using SBN calcination at 600°C for 4 h.

X-ray diffraction patterns were obtained on a Phillips APD 3600 diffractometer. Semiquantitative analyses of the impure RHO samples were obtained by assuming that the samples contain only RHO, chabazite, pollucite, and P_c. The intensities (*I*) of the characteristic reflections (411) for RHO, (401) for chabazite, (400) for pollucite, and (110) for P_c were used in the calculation as follows: %RHO = I[RHO (411)]/[RHO (411)] + I[chab (401)] + I[poll (400)] + I[P_c (110)] × 100. More precise quantitative analyses could not be obtained because of the lack of exact correspondence of the synthesized impurity phases to those contained in the RHO preparations.

Compositional analyses for typical chabazite aggregates and hexagonal platelets of unidentified structure were made using a Hitachi H-600 TEM with an energy-dispersive X-ray (EDX) spectrometer attachment. X-ray intensities were calibrated with chemically analyzed mineral samples of chabazite from Nova Scotia and Pyramid Lake, California, and synthetic ZK-5. Data from at least seven different samples were averaged to obtain Si/Al, Ca/Si, K/Si, and Cs/Si ratios.

Infrared experiments were performed according to the procedure already described (*14, 15*). Internal Lewis acid site concentration was estimated from adsorption of MeCN. External acid site concentrations were obtained by adsorption of pyridine.

Mercury porosimetry was used to measure the exterior surface areas of zeolite preparations. Data were obtained to 60 kpsi using a Micromeritics Model 9200 Autopore. Corresponding surface area measurements using vapor-phase adsorption showed that Hg porosimetry data to 45 kpsi (40 Å) provided a reasonable (within 5–10%) measure of the external surface area. Surface areas for pore dimensions below 40 Å were obtained from vapor-phase adsorption of molecules too large to enter the zeolite framework.

For all of the RHO preparations, the measured surface area for macropores larger than 0.12 μm is 6.8 m^2/g, which agrees with the calculated value based on particle geometry. Thus, there are no macropores larger than 0.12 μm. Most of the preparations have surface area contributions of 30 m^2/g from pores in the range 40–1200 Å, but the lack of other independent methods prohibits assignment of the areas to macroporosity on the RHO surface, faceting of the RHO surface, or contributions from other phases.

Catalytic behavior was evaluated in a U-tube reactor at 250–400°C using a methanol/ammonia mixture at a molar ratio of 1 : 1. Details of the methods of analysis are given in Ref. (*4*). Data were fit to a second-order reaction mechanism described by Keane *et al.* (*1*) which includes three primary series-parallel reactions, two minor disproportionation reactions, and one side reaction. The parameters used to evaluate DMA and TMA selectivities are k_2/k_3 and k_3, respectively, where k_1 has been set to 1 using the following scheme:

$$NH_3 + MeOH \xrightarrow{k_1} MMA + H_2O$$

$$MMA + MeOH \xrightarrow{k_2} DMA + H_2O$$

$$DMA + MeOH \xrightarrow{k_3} TMA + H_2O$$

TABLE 1

Catalytic and IR Properties of Impurities in RHO Preparations

Sample	SV[a] (h^{-1})	T_{90}[b] (°C)	T (°C)	Conv. (%)	DME (%)	DMA (%)	TMA (%)	k_2	k_3	k_2/k_3	I(MeCN) 2330 cm^{-1}	I(pyrB) 1545 cm^{-1}	I(pyrL) 1455 cm^{-1}
A. Gel													
H-gel 0 h DB	0.12–0.23		400	89	15	18	69	37	33	1.1			
H-gel 8 h DB	0.07–0.14		425	89	16	19	66	37	29	1.1			
H-gel 600SB	0.06–0.13	400	400	93	12	25	47	27	34	0.80	0.015	0.008	0.096
H-gel 600SBST	0.06–0.13	400	375	91	13	13	74	29	38	0.78	0.009	0.008	0.071
B. P_c													
H-P_c (A) 600SB	0.01–0.02	>400	400	23	9	18	29	19	41	0.5			
H-P_c (B) 600SB	0.17–0.25	400	400	91	24	14	69	38	75	0.5	<0.001	0.005	0.050
H-P_c (C) 600SB	0.02–0.04		400	52	13			16	26	0.6			
C. Pollucite													
Cs-poll 600DB	0.004–0.008	>425	425	14	4.0	1	76	88	345	0.25			
H,Cs-poll 600DB	1.0–1.4	350	350	93	8.1	14	78	39	256	0.15	0.054	0.059	0.282
H,Cs-poll 600SB (3 μm)	0.004–0.008	>400				Inactive							
H,Cs-poll 600SB											0.067	0.020	0.187
H,Cs-poll 600SBST	0.13–0.25	400	400	89	4.8	31	37	4.0	5.4	0.7	0.000	0.003	0.035
D. Chabazite													
H,Cs,K-chab(A) 600DB	1.0	325	325	93	15	53	18	4.5	1.6	2.7	0.061	0.005	0.037
H,K-chab(B) 600DB	0.05–0.20	400	400	89	6.5	45	19	1.9	1.8	1.1			
H,Cs,K-chab(A) 600SB	0.17–0.33	375	375	90	10.0	32	44	11.0	8.0	1.4	0.032	0.011	0.092
H,Cs,K-chab(A) 600SB/600SBST	0.25–0.33	375	375	87	21.0	28	49	15.0	13.0	1.1	0.013	0.006	0.048
H-chab(A) 500/500DB	1.1	350	350	91	11.0	52	17	4.7	1.5	3.1			
Typical RHO SB	2.7	300	300	90	11.0	57	15	4.4	1.0	5.2	0.20	0.007	0.030
Typical RHO SBST	3.4	300	300	90	3.0	63	8	3.3	0.4	8.8	0.09	0.003	0.027

[a] Space velocity (at 90% MeOH conversion and normalized to 325°C).
[b] Temperature at which 90% MeOH conversion is attained.

Values of $k_2/k_3 > 1$ indicate DMA selectivity to DMA versus TMA, whereas values of $k_2/k_3 < 1$ indicate a product distribution closer to the equilibrium value.

Space velocity (SV), which correlates to catalyst activity, was obtained from the reactant feed rates and catalyst charge. Space velocity data under typical reactor conditions of 90% MeOH conversion, 325°C, 1 : 1 NH_3-to-MeOH feed composition, and 1 atm were used to compare catalyst activities. This basis demonstrates utility in the range of commercially practiced MeOH conversions and feed compositions at typical operating temperatures for H-RHO.

RESULTS

Gel Impurities

Samples of gel calcined using DB, SBN, and SBST conditions showed 90% MeOH conversions only above 375°C as shown in Table 1A. The activity of gel compared to RHO is evidenced by space velocities of ~0.1 h^{-1} compared to typical values of ~3 h^{-1} for H-RHO. Gel is not DMA selective when compared to H-RHO and produces near-equilibrium product distributions with TMA selectivities of 47–74% and $k_2/k_3 \cong$ 0.8. Low MeCN Lewis site populations (0.01–0.02) and high pyridine Lewis site populations (~0.1) were observed.

P_c Impurities

X-ray patterns of NH_4-P_c derived from Na-P_c and the amorphous phases after calcination at 600°C are shown in Fig. 2. Catalytic results for the X-ray amorphous phases from various P_c preparations are shown in Table 1B. All compositions were catalytically similar to the gel samples, being relatively inactive at $T < 400$°C and nonselective toward DMA. These amorphous phases derived from P_c show low concentrations of pyridine Brønsted and Lewis sites and no MeCN Lewis sites.

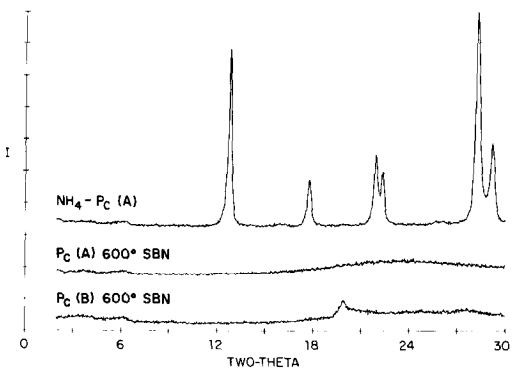

FIG. 2. X-ray diffraction patterns of zeolite P_c before and after shallow-bed calcination.

Pollucite Impurities

The X-ray pattern of the Cs-rich pollucite (Fig. 3) was strong and showed only the reported lines characteristic of pollucite (*16*) (ASTM 25-194). The X-ray patterns of the exchanged, calcined samples were weaker and showed broad lines but are still characteristic of pollucite. In addition two extra lines at 13.8 and 4.26 Å could represent a second phase but more likely indicate a distortion of the 13.8-Å cubic unit cell or a lowering of the *Ia3d* pollucite symmetry.

Catalytic results shown in Table 1C indicate that neither the Cs form of the 0.2- to 0.4-μm pollucite nor the partly NH_4^+-exchanged 1- to 3-μm pollucite is active in methylamine synthesis at $T < 400$°C. However, the 0.2- to 0.4-μm H-pollucite calcined at 600°C DB was active at 350°C (SV = 1.0–1.4 h^{-1}) and TMA selective (78% TMA) with $k_2/k_3 = 0.15$. This sample also showed high pyridine Lewis and Brønsted site populations of 0.282 and 0.059, respectively, 10 times more pyridine Lewis and Brønsted sites than found in a typical H-RHO (*4*). SBST calcination reduced the activity substantially (SV = ~0.2 h^{-1}), eliminated MeCN Lewis sites, and reduced the pyridine Lewis site population to 0.035. This sample was essentially inactive at 325°C with an increased DMA selectivity of $k_2/k_3 = 0.7$.

Chabazite Impurities

Estimates of the relative external surface areas of the RHO crystallites and chabazite aggregates from Hg porosimetry measurements indicate 7–15 and 10–15 m^2/g, respectively. Thus, the chabazite phase, despite the fact that it is a minority phase, provides a significant portion of the external surface area of typical RHO samples.

The compositions of cauliflower-like aggregates from two normal RHO preparations were determined to be $Ca_{0.8}K_{0.5}Cs_{0.3}Al_{8.5}Si_{27.5}O_{72}$ and $Ca_{0.6}Cs_{0.1}Al_{8.2}Si_{27.8}O_{72}$ by TEM-EDX analyses of 10 different aggregates from each preparation. Ca and K impurities in the gel seem to segregate into the chabazite phase. However, Ca and K may only be necessary to nucleate the chabazite crystallites because simply reversing the order of adding reagents can increase the chabazite phase to 50–100% of the total product, even though Ca and K remain as barely detectable impurities.

The H,K,Cs chabazite(A) of composition $[H]_{8.6}K_{0.43}Cs_{0.29}Al_{9.3}Si_{26.7}O_{72}$ and K-chabazite(B) (not analyzed) were calcined under DB, SBN, and SBST conditions. X-ray diffraction patterns (Fig. 4) show that the crystallinity of H-chabazite depends strongly on the calcination conditions of the NH_4-chabazite precursor. Although K-chabazite(B) became amorphous after DB

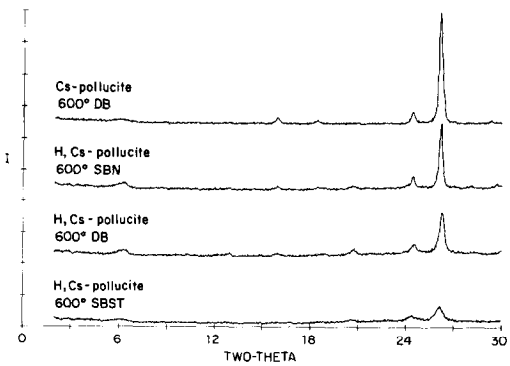

FIG. 3. X-ray diffraction patterns of zeolite pollucite after stagnant deep-bed, deep-bed, and steam calcination.

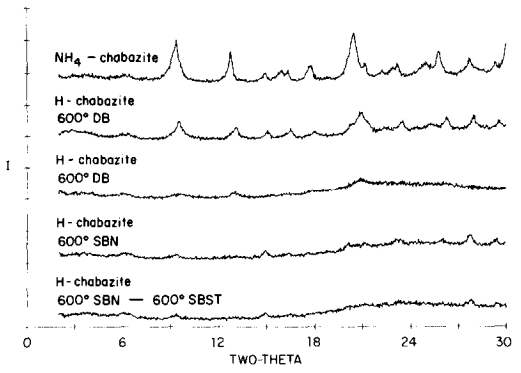

FIG. 4. X-ray diffraction patterns of NH_4-chabazite before and after deep-bed and shallow-bed calcination.

calcination at 600°C, K,Cs-chabazite(A), more analogous to what is found as an impurity in RHO preparations because of the presence of Cs, retained considerable crystallinity after either DB or SBST calcination. This may appear unusual but we have generally observed that amorphitization of zeolites occurs at lower temperatures under SBN conditions than steaming conditions. This is evident for H-RHO where 700°C SBN calcination resulted in 13.2% MeOH sorption and 700°C SBST calcination resulted in 17.6% MeOH sorption.

The crystalline chabazite samples, H,Cs, K-chab(A) 600DB, H,K-chab(B) 600DB, and H-chab 500DB(A) are DMA selective (45–53%; see Table 1D) and are comparable to more highly crystalline mineral chabazites previously described (*3*) and typical DB-calcined H-RHO (*1–4*). These synthetic H-chabazites also have acid site populations similar to those of H-RHO:

	MeCN	pyrB	pyrL
H-chabazite 600DB	0.06	0.005	0.037
H-RHO (typical)	0.1–0.2	~0.005	~0.030

The almost amorphous SBN-calcined materials (see Fig. 4) are nonselective toward DMA and less active than the DB-calcined samples (see Table 1D). The number of MeCN Lewis sites decreases, whereas the number of pyridine Brønsted and Lewis sites increases:

	MeCN	pyrB	pyrL
Chabazite cryst. 600DB	0.06	0.005	0.037
Chabazite amorph. 600SBN	0.032	0.011	0.092
Chabazite amorph. 600SBN/ 600SBST	0.013	0.006	0.048

SBN calcination at 600°C produces more external Brønsted and Lewis sites than DB calcination (~2×), but SBN calcination followed by steaming reduces external Brønsted and Lewis sites to a level similar to that of H-RHO.

Hexagonal Platelet Impurities

In certain RHO preparations, an impurity having hexagonal platelet (HPL) morphology appears. TEM-EDX analysis of 10 different HPL crystals showed their composition to be approximately $Cs_{0.16}AlSi_3O_8$ where charge balance is probably made up by protons. It is not known whether this phase is zeolitic or simply a hydrate.

In a sample concentrated by settling, three prominent peaks appeared in the RHO patterns at 13.6, 3.68, and 3.00 Å. The best indexing of the powder pattern was obtained with a hexagonal unit cell: a = 17.25 Å, c = 12.50 Å, where a was obtained from electron diffraction patterns. The phases $CsAlSi_5O_{12}$ (*17, 18*), $Cs_{0.35}Al_{0.35}Si_{2.65}O_6$ (*19*) and pollucite (*10, 16, 20*) all have cell dimensions with one axis equal to or a multiple of 13.8 Å, so that the structure of the HPL phase may be related to one of these other Cs,Al silicates.

Direct catalytic data on the HPL phase are not available. However, we infer that its catalytic contribution is low because two samples of H-RHO with widely differing amounts of the HPL impurity have only slightly different DMA selectivities.

Impure RHO

Figure 5 shows that DMA selectivity relative to TMA selectivity (k_2/k_3) of impure RHO samples decreases as the total impurity content increases. Because pollucite makes up more than 60% of the total impurity content and because pollucite was

shown either to be inactive or to have low DMA selectivity ($k_2/k_3 < 0.25$), we believe that much of the loss of DMA selectivity results from the presence of pollucite.

DISCUSSION

The inactivity of gel indicates that it does not significantly affect product selectivity for methylamine synthesis over H-RHO. Therefore, stopping RHO crystallizations in the early stages when residual gel is present is not harmful. However, significant quantities of gel would dilute the catalyst and reduce the apparent activity of a sample of RHO with gel impurity. Amorphous impurities resulting from calcination of P_c behave similarly and should not contribute to the methylamine distribution over typical RHO preparations.

Although chabazite is always present in RHO samples, it does not seem to be very important in determining methylamine selectivities. When crystalline, following 500 or 600°C DB calcination, chabazite is DMA selective (DMA/TMA = 53/18%) so that DMA selectivities of chabazite-containing RHO should be only slightly lower than those of chabazite-free RHO. Shallow-bed calcination amorphitizes chabazite, rendering it nonselective toward DMA, but reducing its activity. Therefore, SBN calcination should reduce the activity of H-RHO only slightly.

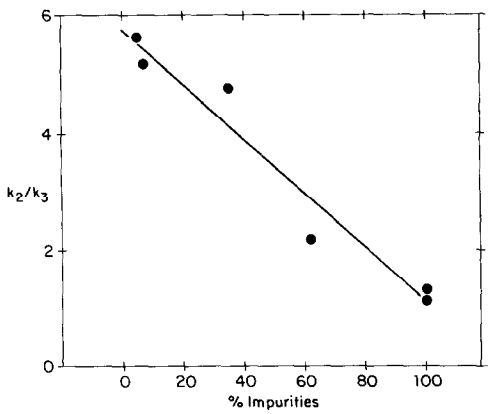

FIG. 5. DMA selectivity (k_2/k_3) of H-RHO/impurity mixtures versus percentage impurity content.

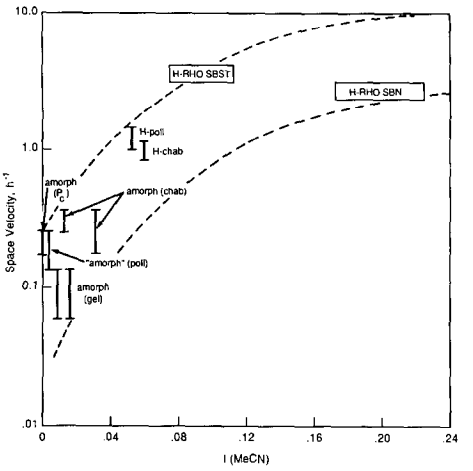

FIG. 6. Catalytic activity of H-RHO and typical RHO impurities versus intensity of 2330 cm^{-1} MeCN band.

The DME yields over chabazite are high (10–20%), but at typical 10% levels in H-RHO, chabazite accounts for only 1–2% DME in a RHO catalyst.

The presence of nonselective, active pollucite impurities can be one of the primary causes of lower DMA selectivities of RHO catalysts calcined under DB conditions. As indicated from the plot of k_2/k_3 versus percentage impurities in Fig. 5, pollucite-rich impurities have increased the TMA selectivity of this H-RHO from 15–20% to about 40–50%, i.e., k_2/k_3 decreases from ~5 to ~1. The semiquantitative XRD analyses result in only approximate impurity contents but they serve to illustrate the point that impurities severely affect DMA and TMA selectivities of the catalyst.

Low MeCN Lewis site populations (0.01–0.02) in amorphous gel and P_c, and steamed pollucite correlate with low activities. Furthermore, a reduction in MeCN Lewis site population by steaming chabazite relative to DB calcination also lowers the activity. Catalyst activity (space velocity) versus I(MeCN) is plotted in Fig. 6 for SBN- and SBST-calcined H-RHO and individual impurity phases. The dashed lines bracket the individual values and indicate a nonlinear relationship where P_c (amorph)

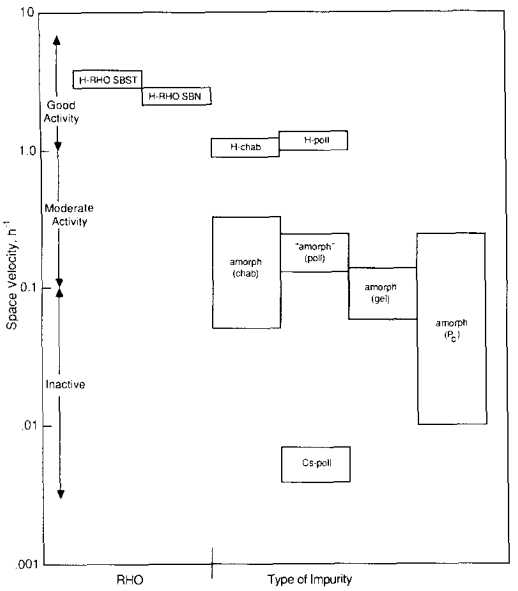

FIG. 7. Catalytic activity of H-RHO and typical RHO impurities ranked in order of decreasing activity.

exhibits only 1/200th of the activity of RHO.

Figure 7 ranks the impurities according to their relative activities. Catalysts are divided into (1) inactive species such as amorphous material from P_c, Cs-pollucite, and gel; (2) moderately active species such as partially amorphous material derived from chabazite and H-pollucite; and (3) active crystalline species such as H-RHO, chabazite, and H-pollucite. In general, steaming is one of the most effective methods of reducing the activities of impurities. This is apparently achieved by destruction of either the crystal structure and/or nonselective surface sites.

The selectivities for DMA relative to TMA formation are ranked in Fig. 8: RHO > chabazite DB $\gg$ amorphous (chabazite) > amorphous (gel) > amorphous (P_c) ~ amorphous (H,Cs-pollucite) > H,Cs-pollucite. The TMA selectivities of the impurities seem to be determined by the relative number of external Lewis sites. DB-calcined H,Cs-pollucite, the most nonselective RHO impurity, exhibits high populations of both external Brønsted and Lewis sites and internal Lewis sites. Low selectivity toward DMA (k_2/k_3 = 0.15) may well result from the Lewis acidity. γ-Al_2O_3, which also has high Lewis acidity, is nonselective toward DMA (*4, 21*).

SUMMARY

RHO zeolite, as synthesized, may contain a variety of other phases: gel, P_c, pollucite, and chabazite. None of these phases after exchange and calcination is as active or selective as H-RHO for the synthesis of dimethylamine from ammonia and methanol. These phases, however, may convert DMA to TMA, thereby lowering the selectivity for a given RHO sample. Calcination, under shallow-bed conditions with flowing nitrogen or steam, converts these phases to relatively inactive amorphous aluminosilicates. Therefore, the DMA selectivity of H-RHO zeolite improves under these calcination conditions because the activity of these secondary, nonselective phases is destroyed. Deep-bed calcination was found to

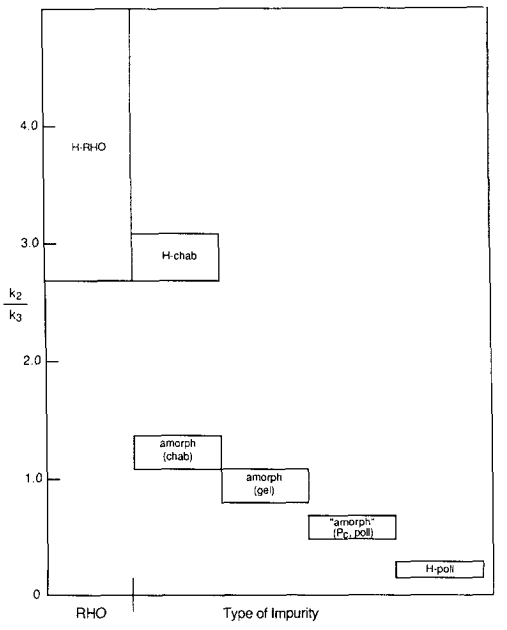

FIG. 8. Relative DMA selectivity of H-RHO and typical RHO impurities ranked in order of decreasing selectivity.

be much less severe and permitted chabazite and pollucite to exist as active phases after calcination.

ACKNOWLEDGMENTS

We thank M. Van Kavelaar for the scanning electron micrographs and I. R. Hartmann for the TEM-EDX analyses.

REFERENCES

1. Keane, M., Jr., Sonnichsen, G. C., Abrams, L., Corbin, D. R., Gier, T. E., and Shannon, R. D., *Appl. Catal.* (1987).
2. Gier, T. E., Shannon, R. D., and Sonnichsen, G. C., U.S. Patent 4,602,112, July 22, 1986.
3. Abrams, L., Gier, T. E., Shannon, R. D., and Sonnichsen, G. C., European Patent Appl. 183, 423.
4. Shannon, R. D., Keane, M., Jr., Abrams, L., Staley, R. H., Gier, T. E., Corbin, D. R., and Sonnichsen, G. C., *J. Catalysis* **113,** 367 (1988).
5. Barrer, R. M., Baynham, J., Bultitude, F. W., and Meier, W. M., *J. Chem. Soc.,* 195 (1959).
6. Barrer, R. M., Bultitude, F. W., and Kerr, I. S., *J. Chem. Soc.,* 1521 (1959).
7. Taylor, A. M., and Roy, R., *Amer. Min.* **49,** 656 (1964).
8. Meier, W. M., and Olson, D. H., "Atlas of Zeolite Structure Types." J. Druck Verlag AG, Zurich, 1978.
9. Baerlocher, C., and Meier, W. M., *Z. Kristallogr.* **135,** 339 (1972).
10. Beger, R. M., *Z. Kristallogr.* **129,** 280 (1969).
11. Robson, H. E., U.S. Patent 3,720,753, March 13, 1973, Example II-2.
12. Kimpe, C. R., *Clay Min.* **7,** 203 (1967).
13. Robson, H. E., U.S. Patent 3,904,738, Sept. 9, 1985, Example I.
14. Fischer, R. X., Baur, W. H., Shannon, R. D., Staley, R. H., Vega, A. J., Abrams, L., and Prince, E., *J. Phys. Chem.* **90,** 4414 (1986).
15. Shannon, R. D., Staley, R. H., and Auroux, A., *Zeolites* **7,** 301 (1987).
16. Sakurai, K., Kato, A., Kuwano, N., and Nagashima, K., *Bull. Chem. Soc. Japan* **45,** 812 (1972).
17. Ito, J., *Amer. Min.* **61,** 170 (1976).
18. Araki, T., *Z. Kristallogr.* **152,** 207 (1980).
19. Annehed, H., and Falth, L., *Z. Kristallogr.* **166,** 301 (1984).
20. Newnham, R., *Amer. Min.* **52,** 1515 (1967).
21. Mochida, I., Yasutake, A., Fujitsu, H., and Takeshita, K., *J. Catal.* **82,** 313 (1983).